Available online at www.sciencedirect.com
ScienceDirect
Trans. Nonferrous Met. Soc. China 35(2025) 653−668
Transactions of Nonferrous Metals Society of China
www.tnmsc.cn

Facile regeneration of spent lithium-ion battery cathode materials via tunable oxidization and reduction strategy

Xue-hu ZHONG[1], Wen-qing QIN[1], Jiang ZHOU[2], Jun-wei HAN[1]

1. School of Minerals Processing and Bioengineering, Central South University, Changsha 410083, China;
2. School of Materials Science and Engineering, Central South University, Changsha 410083, China

Received 29 July 2023; accepted 10 April 2024

Abstract: A tunable oxidization and reduction strategy was proposed to directly regenerate spent $LiFePO_4$/C cathode materials by oxidizing excessive carbon powders with the addition of $FePO_4$. Experimental results indicate that spent $LiFePO_4$/C cathode materials with good performance can be regenerated by roasting at 650 °C for 11 h with the addition of Li_2CO_3, $FePO_4$, V_2O_5, and glucose. V_2O_5 is added to improve the cycle performance of regenerated cathode materials. Glucose is used to revitalize the carbon layers on the surface of spent $LiFePO_4$/C particles for improving their conductivity. The regenerated V-doped $LiFePO_4$/C shows an excellent electrochemical performance with the discharge specific capacity of 161.36 mA·h/g at 0.2*C*, under which the capacity retention is 97.85% after 100 cycles.
Key words: spent lithium-ion batteries; direct regeneration; cathode materials; roasting; circular economy

1 Introduction

Olivine lithium iron phosphate ($LiFePO_4$/C) batteries are widely used for their excellent thermal stability, long cycle life, and cost-effectiveness [1]. The global shipment of these power batteries was 957.70 GW·h in 2022, an increase of 70.30% over 2021, and it will increase to 1290.80 GW·h in 2030 [2]. $LiFePO_4$/C battery is one of the most important lithium-ion batteries, taking China as an example, the production of $LiFePO_4$/C batteries was 332.40 GW·h in 2022, accounting for 60.90% of the total power batteries produced. The large-scale application of $LiFePO_4$/C batteries contributes significantly to reducing global carbon dioxide emissions and promoting environmental protection [3,4]. However, massive spent $LiFePO_4$/C batteries containing heavy metals and organic electrolytes, which are not environment-friendly and can jeopardize human health [5], have been produced due to the limited lifespan of $LiFePO_4$/C batteries (i.e., 5−8 a (1 a=1 year)) [6]. In 2021, approximately 2.94×10^5 t of spent lithium-ion batteries (LIBs) were produced in China, most of them are spent $LiFePO_4$/C and $Li(Ni_xCo_yMn_z)O_2$ batteries, and this value is predicted to quickly increase up to 2.312×10^6 t in 2026 [7]. Moreover, as the global LIB market continues to grow, there is a looming shortage of critical metals, including lithium (Li). Consequently, the recycling of spent LIBs has become an urgent environmental and resource management issue that requires immediate attention [8].

The recycling process of spent LIBs primarily involves battery collection, the pretreatment and regeneration of active materials and recycling valuable metals [9]. Among them, the regeneration of cathode active materials (CAMs) is critical to spent LIBs recycling because CAMs are the most valuable part of spent batteries [9,10]. Hydro-metallurgical and pyrometallurgical processes are

Corresponding author: Jun-wei HAN, E-mail: hanjunwei@csu.edu.cn
DOI: https://doi.org/10.1016/S1003-6326(24)66706-3

the conventional methods of recovering valuable metals from spent LIBs [11,12]. The pyro-metallurgical process smelts the valuable metals in CAMs to metal alloys with a reductant at high temperatures (800−1000 °C), leaving the critical lithium in slags [13]. The most widely used hydrometallurgical process digests CAMs with organic or inorganic acid (e.g., HCl, H_2SO_4, and methyl sulfonic acid), recovers valuable metals in the form of pure metals or metal hydroxides, and is then followed by purification steps (precipitation or solvent extraction) [14−16]. However, both of these technologies face challenges in efficiently separating and recovering targeted metals in an economically viable manner [17,18].

Another strategy, which regenerates CAMs directly from the spent CAMs and thus avoids the separation of multiple metal ions, has been recently examined to be more economically competitive and have less greenhouse gas emissions than traditional recycling processes that generate elemental products [19]. This strategy maximizes the reusability of metals from spent LIBs and obtain high value-added products [20,21]. More importantly, this concept makes it profitable for the recovery of the little valuable metals-containing spent $LiFePO_4$/C batteries, one of the most widely used LIBs [22]. However, different impurities such as Cu, Ni, Mg, Al, C and Fe may mix into the recovered CAMs for the complicated components of spent LIBs [23], leading to the inferior electrochemical properties of the regenerated CAMs. Although the direct regeneration method for spent $LiFePO_4$/C batteries has high potential, the removal of impurities, especially carbon, remains a problem [24]. The carbon content should be controlled in the regenerated $LiFePO_4$/C materials, but carbon is produced as a result of polyvinylidene fluoride (PVDF) during the recycling of spent $LiFePO_4$/C batteries. The efficient removal of impurities, especially for carbon powder, is difficult and complicated, thereby impeding the industrial application of the direct regeneration of spent LIBs.

In this study, a tunable oxidization and reduction strategy was developed to directly regenerate spent $LiFePO_4$/C in the presence of carbon powder impurity. The carbon content in the regenerated $LiFePO_4$/C was regulated and controlled using an oxidizing agent ($FePO_4$) through redox reactions, without affecting the regeneration process. The reducing agent glucose ($C_6H_{12}O_6$, Glc) was used to revitalize the carbon layers on the surface of the spent and newly formed $LiFePO_4$/C, thereby improving the conductivity. By carefully controlling and regulating the dosages of oxidant and reductant, the spent $LiFePO_4$/C could be easily and directly regenerated. The effects of $FePO_4$, Li_2CO_3, and Glc on the direct regeneration process were studied in detail. The optimal dosages of NiO, Al_2O_3, MgO, Nb_2O_5, V_2O_5 and their effects on the cycle performance of the regenerated $LiFePO_4$/C were thoroughly explored. Economic analysis was also performed on the direct regeneration process. This approach has potential application in recycling other types of CAMs, such as $LiMn_2O_4$ and $LiNi_xCo_yMn_zO_2$ with proper modifications.

2 Experimental

2.1 Materials

Spent $LiFePO_4$ batteries were acquired from a battery disposal factory in Hunan Province, China. The average working voltage and elapsed time of the spent $LiFePO_4$/C batteries are 3.38 V and 6 a, respectively. The proportions of different parts in the spent $LiFePO_4$ batteries are shown in Table S1 in Supporting Materials (SM). The spent $LiFePO_4$/C batteries were disposed by efficient crushing without discharging and low-temperature volatilization. The separators, shells, Al and Cu foils were selected and obtained through pneumatic separation, catalytic pyrolysis and color sorting, respectively [25−27]. The active materials were further separated by green and industrialized flotation, and the spent CAMs were obtained (Fig. S1 in SM).

The X-ray fluorescence analysis of the recovered CAMs indicated that the main elements present were Fe, O, P, F, V, Al, Cu, and P, with almost no other metals found (Table S2 in SM). Inductively coupled plasma-optical emission spectroscopy (ICP-OES) and atomic absorption spectroscopy analyses show that the Li, Cu, Al, V, and Fe contents are 2.06, 0.06, 0.12, 0.91, and 34.29 wt.%, respectively. The combustion method revealed a carbon content of 15.67 wt.% in the recovered CAMs, and the phosphorus molybdenum blue method indicated a phosphorus content of 19.34 wt.%. The SEM and X-ray diffraction (XRD)

results demonstrated that the recovered CAMs mainly consisted of $LiFePO_4$ and C. The white particles observed in the SEM spectra were about 100 μm in size, mainly consisting of O, P, and Fe, while the dark particles were approximately 10 μm in size, mainly consisting of O and C (Figs. S2(a−d) in SM). Hence, the white particles were primarily $LiFePO_4$/C, while the dark particles were mainly C.

The chemical reagents used in this study included analytical-grade lithium carbonate (Li_2CO_3), ferric phosphate ($FePO_4$), Glc, nickel oxide (NiO), magnesium oxide (MgO), aluminum oxide (Al_2O_3), vanadium pentoxide (V_2O_5) and niobium pentoxide (Nb_2O_5). All the chemicals were purchased from Macklin.

2.2 Material characterization

Powder XRD patterns were recorded on a Rigaku TTR-III diffractometer using Cu K_α radiation (λ=1.5418 Å, 50 kV and 100 mA). The metal elements contents were determined via ICP-OES (PerkinElmer Optima 7300 V, America). The surface properties of the samples were analyzed via XPS (Thermo Fisher-VG Scientific, ESCALAB250Xi). The XPS data were analyzed using the Avantage software 5.52. The particle size distributions of the samples were analyzed using a Mastersize 2000 laser particle size analyzer. The morphological properties and the elemental distributions on the surface of the samples were detected via SEM (JEOL, JSM−6490LV) coupled with energy dispersive spectrum (EDS, JEOLJSM−6490LV). Transmission electron microscopy (TEM, JEM−2100F) was employed to record the scanning transmission electron microscopy, high-resolution TEM (HRTEM) and selected area electron diffraction (SAED) images. The regeneration process was analyzed by TGA−FTIR−MS through TGA (PerkinElmer, TGA8000) in combination with FTIR (Nicolet IS10) and mass spectrometry (NETZSCH QMS 403). About 30 mg of the regeneration raw materials were evenly spread at the bottom of the alumina crucible at a heating rate of 10 °C/min from 30 to 650 °C. The test was carried out under high purity nitrogen atmosphere with a gas flow rate of 50 mL/min. The infrared resolution was 4 cm^{-1}, and the number of scans per minute was 32. This regeneration process was investigated by in situ SEM (FEI-Quanta FEG 650) and in situ XRD (Xpert Pro MPD) under pure Ar atmosphere.

2.3 Tunable oxidizing and reducing experimental procedures

Certain amounts of lithium source (Li_2CO_3), iron source (Oxidant: $FePO_4$), organic carbon source (Glc), and metal oxides and the recovered CAMs were pulverized and mixed using a planetary ball mill (YXQM−2L, MITR) at various rotational speeds (400−700 r/min), grinding time (3−7 h), and power-to-ball mass ratios (1∶10−1∶25) with anhydrous ethanol as the dispersing liquid. After being dried in a vacuum oven at 110 °C for 24 h, the ground materials were placed in a well-type electric resistance furnace under the protection of high purity Ar for regeneration. The effects of the feeding ratio of different components, the roasting temperature and time were investigated.

2.4 Electrochemical measurements

The electrochemical performance tests were carried out to investigate the superiority of the regenerated materials. According to the mass ratio of 8∶1∶1, certain amounts of regenerated $LiFePO_4$/C, PVDF, and acetylene black (Super-P) were weighed and evenly mixed with the regenerated materials in agate mortar. Then, N-methyl-2-pyrrolidone was dropped into the mixture to make an uniform slurry. The slurry was coated on the surface of the Al foil and then placed in a vacuum drying oven at 120 °C for 24 h. The half-cells were assembled in the glove box. The electrolyte used was composed of 1 mol/L of $LiPF_6$ dissolved in solvent at the volume ratio of EC∶DEC∶PC=1∶1∶1. The galvanostatic charge−discharge tests of half-cells were carried out with the Neware test system. The test temperature was controlled at room temperature, and the cut-off voltage was 2.0−4.0 V. The rate performance was tested at different electric current densities. The cyclic voltammetry (CV) test voltage range was 2.0−4.0 V with 0.1 mV/s as the scanning speed. Electrochemical impedance spectroscopy (EIS) tests were operated using Auto-Lab. The frequency range was 0.01 Hz−100 kHz and the amplitude was 5 mV.

3 Results and discussion

3.1 Regeneration of spent $LiFePO_4$/C cathode materials

3.1.1 Tunable oxidization and reduction strategy

The ICP-OES tests reveal that the molar ratio

of Li/Fe is 0.48 in the spent $LiFePO_4$/C (chemical formula: $Li_{0.48}FePO_4$/C), indicating a significant loss of Li in the spent $LiFePO_4$/C materials, which can potentially result in the poor electrochemical performance of the batteries [28,29]. Previous studies demonstrated that the lost Li can be replenished within the spent $LiFePO_4$/C particles through carbon-thermal reduction, allowing for the recovery of the embodied energy in the electrode active materials. This simple process requires less energy and chemical input than producing new $LiFePO_4$/C, because the chemical break down of the $LiFePO_4$ crystal structure is avoided [30,31]. However, the presence of impurities, particularly the excessive C (15.76 wt.%) in the recovered CAMs still negatively affects the regenerated $LiFePO_4$/C.

To address this issue, a tunable oxidation and reduction strategy was proposed for the direct regeneration of spent $LiFePO_4$/C cathode material. The initial specific discharge capacity of the recovered $LiFePO_4$/C material is 71.62 mA·h/g, which is much lower than that of the new $LiFePO_4$/C (~161 mA·h/g), and the charge−discharge efficiency greatly decreases after 50 cycles (Figs. S2(e, f) in SM). Therefore, it should be further regenerated. The mixture of spent $LiFePO_4$/C, $FePO_4$, Li_2CO_3, and Glc was first ground to the appropriate particle size [32,33]. As shown in Fig. S3 in SM, the half-content diameter (D50) and volume average particle diameter (D[4,3]) of the ground materials are 1.045 and 2.546 μm, respectively. Regenerated $LiFePO_4$/C was then obtained after reacting at the designated temperature and time.

The effect of C and Fe contents, which is determined by the feeding molar ratio of C/Fe, on the electrochemical performance of the regenerated $LiFePO_4$/C was investigated. Figures S4(a−e) in SM show that the initial specific discharge capacity of the regenerated $LiFePO_4$/C increases from 139.01 to 158.14 mA·h/g at 0.1C (1C=170 mA/g) as the C/Fe molar ratio increases from 1.5:1 to 2:1. However, it starts to decrease when the C/Fe molar ratio exceeds 2:1. The regenerated $LiFePO_4$/C contains 3.82 wt.% C at C/Fe molar ratio of 2:1, and its discharge specific capacity (158.14 mA·h/g) is significantly higher than that of the spent $LiFePO_4$/C (71.62 mA·h/g). This result suggests that the direct regeneration process can enhance the electrochemical capacity of spent $LiFePO_4$/C and reduce the C content. However, the optimized regenerated $LiFePO_4$/C only exhibits a capacity retention of 58.62% after 100 cycles at 0.2C, and the coulombic efficiencies are not satisfied (Fig. S4(f) in SM).

The C/Glc and Li/Fe molar ratios also have notable effects on the carbon layer on the surface of $LiFePO_4$/C and the crystal structure of $LiFePO_4$/C [34]. Therefore, the effects of the C/Glc and Li/Fe molar ratios were further studied. The initial specific discharge capacity of the regenerated $LiFePO_4$/C was 79.38 mA·h/g at 0.1C without the addition of Glc. This value significantly increased to 134.81 mA·h/g at 0.1C with the addition of Glc (C/Glc molar ratio of 360∶1), and further increase of the Glc content decreased the discharge capacities, with a value of 113.57 mA·h/g at the C/Glc molar ratio of 60:1 (Figs. S5(a−f) in SM). However, the capacity retention was only 40.84% after 100 cycles at 0.2C, which is much lower than that at the C/Glc molar ratio of 180:1 (Fig. S4(c) in SM), and the coulombic efficiencies remained unsatisfied (Fig. S5(f) in SM), which may be due to the poor reversibility of the regenerated $LiFePO_4$/C materials. The initial specific discharge capacity of the regenerated $LiFePO_4$/C decreased from 149.45 to 101.23 mA·h/g at 0.1C as the Li/Fe molar ratio increased from 0.95∶1 to 1.3∶1 (Fig. S6 in SM). From these results, optimized C/Fe, C/Glc and Li/Fe molar ratios for the regeneration were found to be 2∶1, 180∶1 and 1∶1, respectively. However, the capacity retention of the regenerated $LiFePO_4$/C remained extremely low, requiring further improvement.

3.1.2 Cycle performance evolution by doping with metal oxide

Metal oxide doping is an efficient and widely used method for improving the cycling performance of $LiFePO_4$/C materials [35]. Hence, the effects of different metal oxides on the electrochemical performance of regenerated $LiFePO_4$/C were investigated to find the best metal oxide for the doping of our system. First, several typical divalent and trivalent metal oxides (MgO, NiO, and Al_2O_3) were investigated. According to the results of the galvanostatic charge−discharge tests (Figs. S7−S9 in SM), the cycle performance of the regenerated $LiFePO_4$/C was improved by adding these metal oxides. But unfortunately, the discharge specific

capacities were less those without metal oxides with the optimal dosages of MgO (Fig. S7 in SM), NiO (Fig. S8 in SM), and Al_2O_3 (Fig. S9 in SM) of 2, 0.1, and 0.1 wt.%, respectively.

To enhance the electrochemical performance of $LiFePO_4$/C, we investigated the use of rare metal oxide doping. This strategy involves the addition of rare metal oxides, such as Nb_2O_5 and V_2O_5, which have high electronic charges, large ion radii, and strong self-polarization ability [36,37]. The initial specific discharge capacity of the regenerated Nb-doped $LiFePO_4$/C increased from 75.59 to 148.16 mA·h/g at 0.1*C* when the dosage of Nb_2O_5 increased from 0.1 to 2 wt.%. However, further increase in the Nb_2O_5 content led to a decrease in the specific discharge capacity. The capacity retention of the 2 wt.% Nb-doped regenerated $LiFePO_4$/C was 75.58% after 100 cycles at 0.2*C* (Fig. S10 in SM). Meanwhile, doping V_2O_5 increased the initial specific discharge capacity (159.40 mA·h/g at 0.1*C*, which is close to that of commercial materials) and improved the capacity retention (89.96% after 100 cycles at 0.2*C*) at a low doping content of 0.1 wt.% (Fig. S11 in SM). Therefore, V_2O_5 was selected for further experiments.

To optimize the electrochemical performance of the V-doped $LiFePO_4$/C cathode materials, different regeneration conditions were studied, specifically the roasting time and the temperature. Figure S12 in SM demonstrates that the initial specific discharge capacity increased from 43.17 to 130.30 mA·h/g at 0.1*C* when the roasting time increased from 7 to 10 h. However, extending the roasting process to 12 h impaired the performance. The capacity retention of V-doped regenerated $LiFePO_4$/C roasted for 10 h was 92.69% after 100 cycles at 0.2*C*. Roasting temperature also poses significant effects on the electrochemical performances of the regenerated material. As shown in Figs. S13(a−c) in SM and Fig. 1(a), the initial specific discharge capacity of the regenerated V-doped $LiFePO_4$/C reached the maximum of 165.67 mA·h/g at 0.1*C* when the roasting temperature was 650 °C. This high specific capacity may be attributed to the reversible redox reaction between the lithium ions in the electrolyte and the exfoliated graphene flakes [38].

Specific discharge capacity slightly decreased to 161.36 mA·h/g at 0.2*C*, and the capacity retention

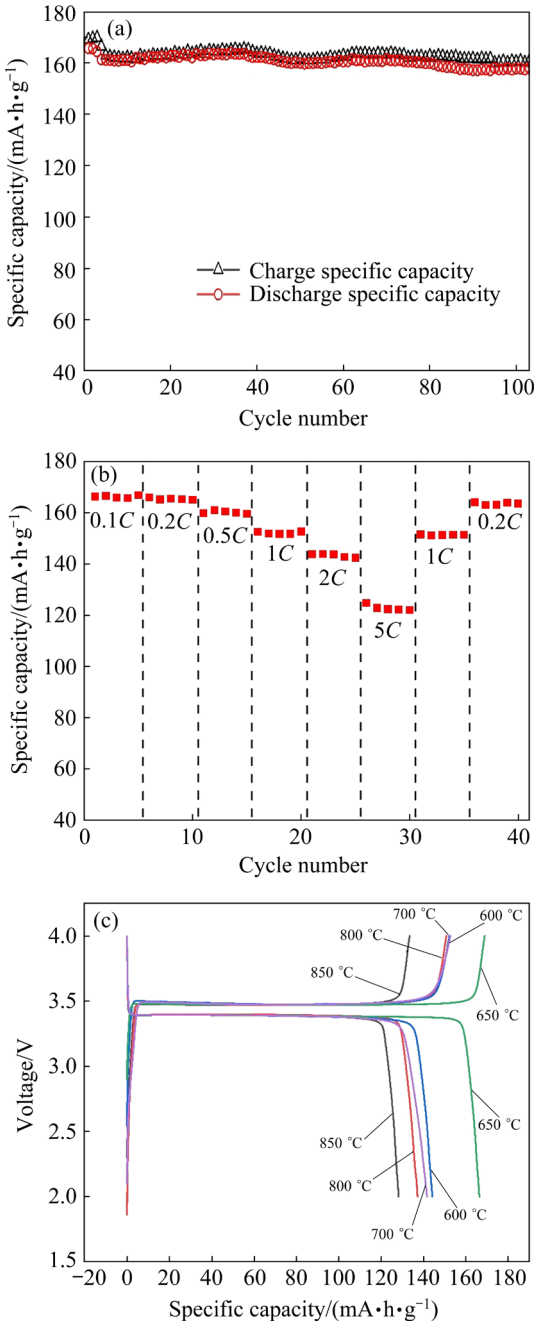

Fig. 1 (a) Cycle performance of V-doped regenerated $LiFePO_4$/C (regenerated at C/Glc molar ratio of 180:1, C/Fe molar ratio of 2:1, Li/Fe molar ratio of 1:1, 0.1 wt.% V_2O_5 in ground materials, roasting time 11 h, the first three cycles were tested at 0.1*C*, and the rest were at 0.2*C*); (b) Rate performance of V-doped regenerated $LiFePO_4$/C materials; (c) Galvanostatic initial charge−discharge curves of V-doped regenerated $LiFePO_4$/C at different roasting temperatures

of the V-doped regenerated $LiFePO_4$/C roasted at 650 °C was 97.85% after 100 cycles at 0.2*C* (Fig. 1(a)). The V-doped regenerated $LiFePO_4$/C has a long and stable charge−discharge platform

(Fig. 1(c)), and the respective discharge specific capacities at 0.5*C*, 2*C*, and 5*C* were 160.51, 142.75, and 122.36 mA·h/g, respectively (Fig. 1(b)), indicating that the discharge specific capacity of the V-doped regenerated $LiFePO_4$/C is nearly the same as that of commercial materials at high discharge rates. Combustion methods indicate that the content of C (3.29 wt.%) regenerated under this condition is nearly the same as the commercial $LiFePO_4$/C [39]. Therefore, the adverse impacts of carbon impurities on the regenerated $LiFePO_4$/C are successfully eliminated by tunable oxidization and reduction and metal oxide doping.

The addition of $FePO_4$, Glc, Li_2CO_3, and V_2O_5 is important for improving the electrochemical performance of regenerated $LiFePO_4$/C materials. The optimal regeneration conditions are as follows: C/Glc, C/Fe and Li/Fe molar ratios being 80∶1, 2∶1, and 1∶1, respectively, 0.1 wt.% V_2O_5 in the ground materials, roasting under Ar for 11 h, 650 °C. Most of the metal oxides (MgO, NiO, Al_2O_3, Nb_2O_5 and V_2O_5) are beneficial to improving the cycle performance. However, the discharge specific capacity sharply decreases when the content of metal oxide exceeds 3 wt.%. Therefore, the amount of metal oxides in spent $LiFePO_4$/C should be minimized, and the carbon impurities in spent $LiFePO_4$/C can be controlled and regulated through a tunable oxidization and reduction strategy.

3.2 Characteristics of regenerated materials

3.2.1 Regeneration of electrochemical properties

CV and EIS techniques were employed to evaluate the electrochemical properties of spent and regenerated $LiFePO_4$/C. In the CV curves (Figs. 2(a−c)), the pair of redox peaks at 3.19 and 3.78 V corresponds to two distinct phase transition reactions during the cycles. The CV curves of the V-doped regenerated $LiFePO_4$/C demonstrate better repeatability (Fig. 2(c)) than those of the other materials (Figs. 2(a, b)), indicating that the regeneration process significantly improved the

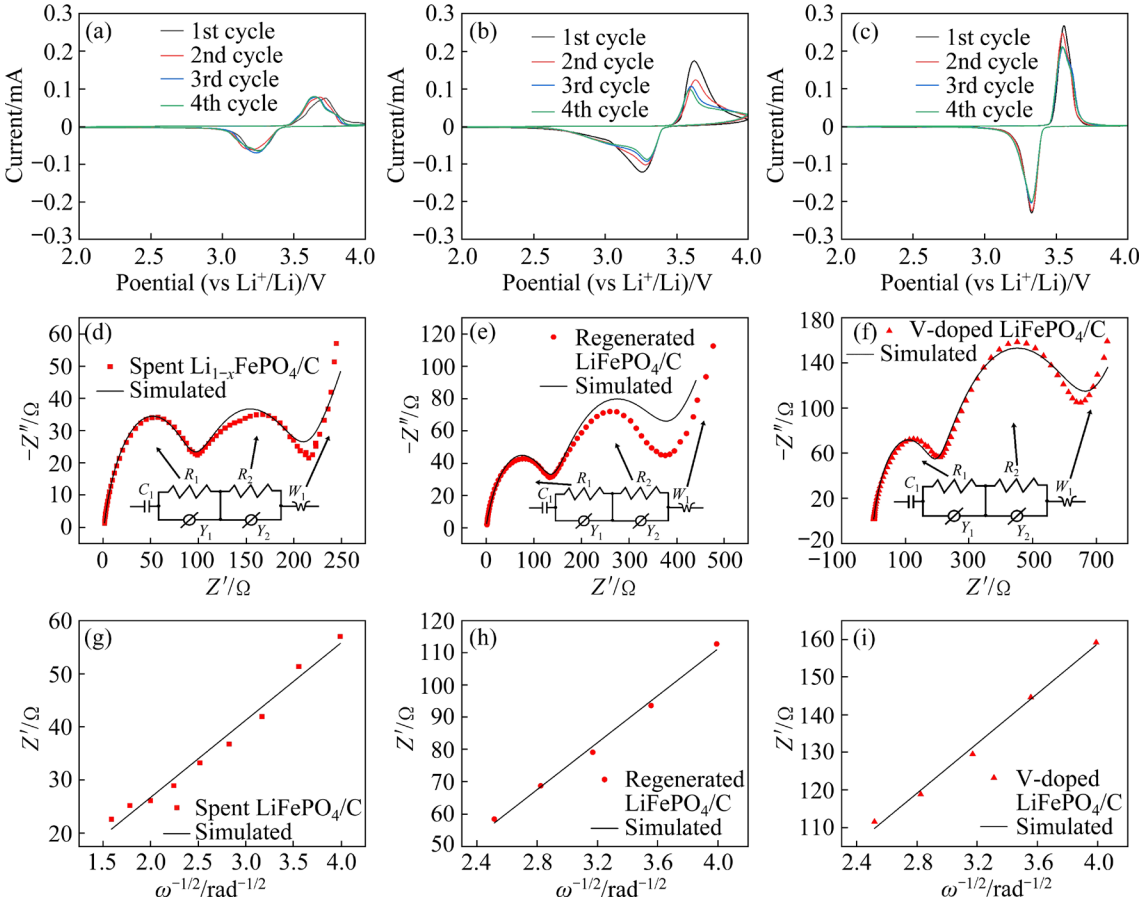

Fig. 2 CV curves of spent $LiFePO_4$/C (a), regenerated $LiFePO_4$/C (b), and V-doped regenerated $LiFePO_4$/C (c); Nyquist plots of spent $LiFePO_4$/C (d), regenerated $LiFePO_4$/C (e), and V-doped regenerated $LiFePO_4$/C (f); Relationship between Z' and $\omega^{-1/2}$ in low-frequency region of spent $LiFePO_4$/C (g), regenerated $LiFePO_4$/C (h), and V-doped regenerated $LiFePO_4$/C (i)

reversibility of the spent $LiFePO_4$/C, which is consistent with the galvanostatic charge−discharge test results (Fig. S2(e) in SM, Fig. 1(b), and Fig. S4(c) in SM). EIS, an important method for evaluating the diffusion coefficient of lithium ions, was used to investigate the changes in lithium-ion transfer during the regeneration process. The radii of the semicircle in the high-frequency (R_1) and mid-frequency (R_2) regions on the real impedance (Z') axis correspond to the surface film and the charge transfer resistance, respectively (Figs. 2(d−f)) [40,41]. The linear portion at low frequency contains information on lithium-ion diffusion as described by the Warburg impedance (Figs. 2(d−f), W_1) [37] and is calculated using as follows:

$$D=\frac{R^2T^2}{2A^2n^4F^4C^2\sigma^2} \quad (1)$$

where D is the diffusion coefficient of lithium ions, R is the molar gas constant, T is the thermodynamic temperature, A is the surface area of the cathode, n is the number of electrons per molecule during oxidization, F is the Faraday constant (96486 C/mol), C is the concentration of lithium-ion, and σ is the Warburg factor which is calculated using Eq. (2):

$$Z'=R_1+R_2+\sigma\omega^{-1/2} \quad (2)$$

where ω is the angle frequency. The linear fitting of Z' versus $\omega^{-1/2}$ is shown in Figs. 2(g−i), from which the slope σ can be obtained. From Eqs. (1) and (2), the lithium-ion diffusion coefficients of the spent and regenerated $LiFePO_4$/C were calculated to be 2.79×10^{-12} and 4.45×10^{-13} cm^2/s, respectively. This value increased to 5.55×10^{-13} cm^2/s for the V-doped regenerated $LiFePO_4$/C, which had a smaller cell volume than that without V, and the lithium-ion diffusion coefficients of the V-doped regenerated $LiFePO_4$/C were nearly the same as that of the commercial $LiFePO_4$/C [42].

3.2.2 Evolution of carbon layer and surface compositions

HRTEM analysis was conducted on the spent $LiFePO_4$/C, the regenerated $LiFePO_4$/C, and the V-doped regenerated $LiFePO_4$/C to investigate the changes in carbon layer and crystal structure during the regeneration process. The spent $LiFePO_4$/C exhibited irregular and rough particle surfaces with attached impurities, some of which caused surface damage (Fig. 3(a)). The carbon layers were unevenly coated with a thickness ranging from 1.365 to 4.513 nm (Fig. 3(b)), and the lattice fringes appeared fuzzy and unclear (Fig. 3(c)). These deficiencies significantly contributed to the decline in discharge specific capacity of the spent $LiFePO_4$/C. The regenerated $LiFePO_4$/C particles displayed regular and elliptical shapes, with uniformly coated surface carbon layers measuring approximately 1.818 nm and clear lattice fringes (Figs. 3(d−f)). The V-doped regenerated $LiFePO_4$/C particles were also elliptical in shape, while the carbon layers on their surface exhibited increased thickness with good uniformity (about 2.618 nm). The lattice fringes were highly distinct, and the crystal plane spacings (i.e., (111) and (210)) of the V-doped regenerated $LiFePO_4$/C were nearly identical to those of the standard PDF card (3.482 and 3.917 Å), as evidenced by the clear diffraction pattern and the visible crystal plane (Figs. 3(g−i)). The TEM results indicate that this direct regeneration method effectively revitalizes the damaged crystal structure and ensures the uniform redistribution of the coated carbon layer with an appropriate thickness.

3.2.3 Evolution of surface properties

To better understand the mechanism of the electrochemical performance improved by tunable oxidization and reduction direct regeneration and metal oxide doping, the evolution of the surface compositions was investigated by XPS (the results were analyzed by referring to the NIST XPS Database) [42]. Six elements (V, Fe, O, C, Li, and P) were mainly detected on the surfaces of the spent, regenerated and V-doped regenerated $LiFePO_4$/C, as shown in Fig. 4(a), Fig. S15(a) in SM, and Fig. 4(f), respectively. The C-containing compounds on the surfaces of these three $LiFePO_4$/C materials mainly consisted of C (284.80 eV), with the rest in the form of hydrocarbons (C—H, 285.89 eV) and carbon oxides (C—O, 286.79 eV) possibly due to the incomplete thermal decomposition of Glc or PVDF (Figs. 4(b, g) and Fig. S15(b) in SM). The O-containing compounds on the surfaces of the spent $LiFePO_4$/C mainly consisted of carbon oxides (C—O, 531.87 eV), and the rest were mainly in the form of —COO (533.52 eV) and P—O (534.35 eV) (Fig. 4(c)). Unlike the spent material, the O-containing compounds on the surfaces of the

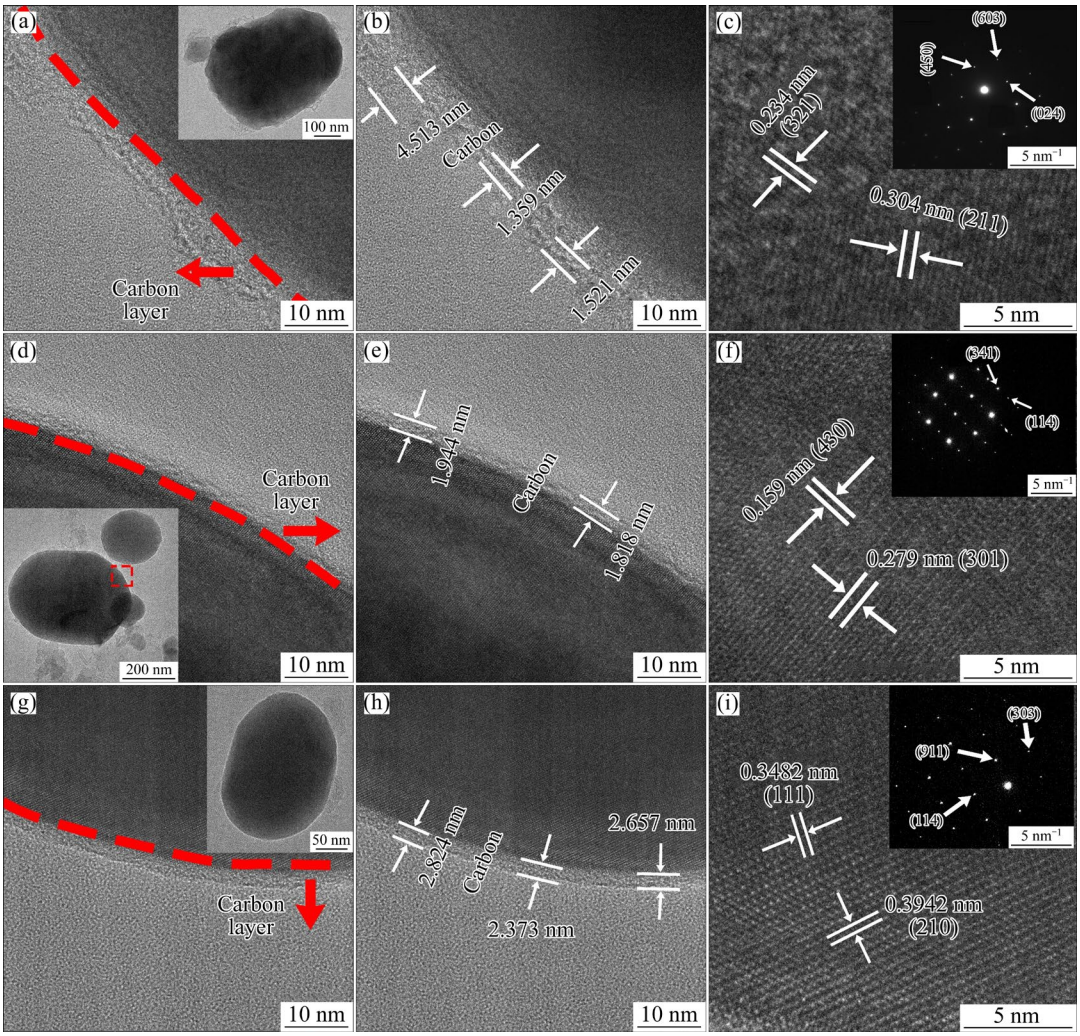

Fig. 3 (a, b) TEM images of spent $LiFePO_4$/C; (c) Selected area electron diffraction (SAED) image of spent $LiFePO_4$/C; (d, e) TEM images of regenerated $LiFePO_4$/C; (f) SAED image of regenerated $LiFePO_4$/C; (g, h) TEM images of V-doped regenerated $LiFePO_4$/C; (i) SAED image of V-doped regenerated $LiFePO_4$/C

regenerated $LiFePO_4$/C were mainly phosphoric-oxygenic compounds (P—O, 531.77 eV), and the rest were in the form of C—O (533.19 eV) and —COO (534.17 eV) (Fig. S15(c) in SM). The O-containing compounds on the surfaces of the V-doped regenerated $LiFePO_4$/C were mainly phosphoric-oxygenic compounds (P—O, 531.37 eV), and the rest were in the form of C—O (532.79 eV) (Fig. 4(h) in SM), indicating that the oxidative species decreased during the regeneration. The V-containing compounds on the surfaces of the spent and regenerated $LiFePO_4$/C were mainly composed of V_2O_5 (517.68 and 517.34 eV) (Fig. 4(e) and Fig. S15(e) in SM), while V—C (523.19 eV) and V_2O_3 (515.89 eV) were clearly observed for V-doped $LiFePO_4$/C in addition to V_2O_5 (517.18 eV) (Fig. 4(j)). This observation demonstrates that the addition of V_2O_5 can promote its reactions with $LiFePO_4$/C. The Fe-containing compounds on the surfaces of spent $LiFePO_4$/C are mainly in the form of Fe_2O_3 (711.26 and 724.44 eV) and the rest was $FePO_4$ (714.55 and 727.74 eV) (Fig. 4(d)), implying that some of the Fe^{2+} on the surfaces of $LiFePO_4$/C was oxidized to Fe^{3+} during the multiple cycles, which is not beneficial to the electrochemical performance of $LiFePO_4$/C [43]. By contrast, the major component of the Fe-containing compounds on the surfaces of regenerated $LiFePO_4$/C and V-doped regenerated $LiFePO_4$/C is Fe—O (Fig. 4(i) and Fig. S15(d) in SM). The disappearance of Fe_2O_3 reveals that the direct regeneration process can revitalize the surface composition and eliminate the detrimental effects of the changed surface properties.

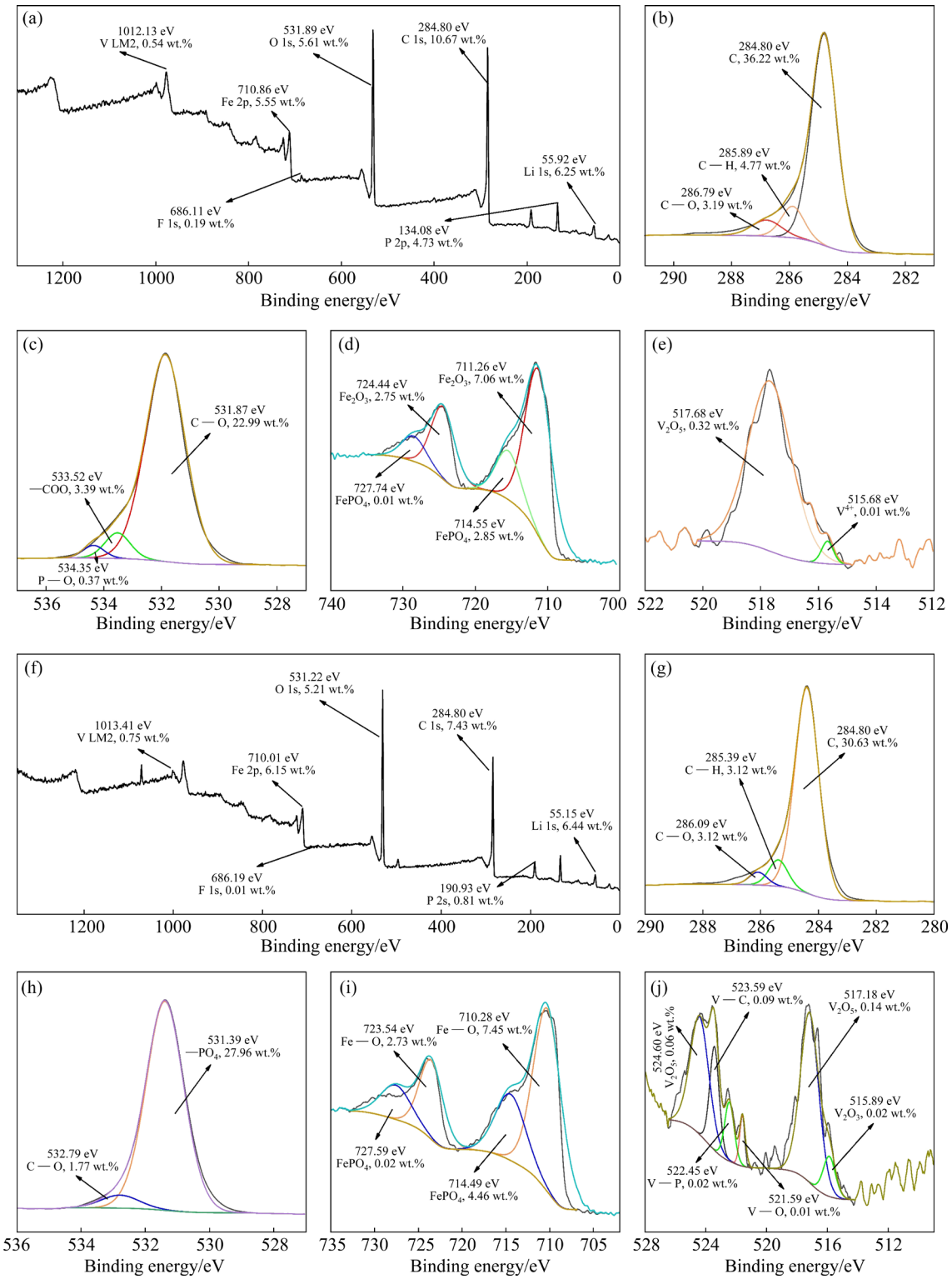

Fig. 4 XPS analysis results of spent (a−e) and V-doped regenerated (f−j) $LiFePO_4$/C: (a, f) XPS survey spectrum; (b, g) C 1s; (c, h) O 1s; (d, i) Fe 2p; (e, j) V 2p

3.3 Mechanism of regeneration

3.3.1 In situ analysis results of regeneration process

To gain a deeper understanding of the reaction mechanism, TGA−FTIR−MS experiments were conducted to analyze the roasting products during the regeneration process. The MS spectra reveal the production of two gases: H_2O (mass-to-charge ratio of (m/z) 18) and CO_2 (mass-to-charge ratio of 44) (Fig. 5(a)). The intensity of CO_2 reached the peak at approximately 290 °C, while the intensity of H_2O

was significantly lower throughout the regeneration process (Fig. 5(b)). The rapid mass loss observed between 300 and 400 °C can be primarily attributed to the thermal decomposition of Glc. Subsequently, a distinct endothermic peak was detected at 420.92 °C, which is likely associated with the formation of $LiFePO_4$/C (Fig. 5(c) and Reaction (3)) [44]. The FTIR spectra show absorption peaks in the wavenumber range of 2408−2269 and 3425−3744.9 cm^{-1}, corresponding to CO_2 and H_2O, respectively, during the regeneration process (Fig. 5(d)). The CO_2 intensity reached its maximum at around 300 °C, while the intensity of H_2O remained lower than that of CO_2. When the temperature exceeded 450 °C, only the absorption peaks of CO_2 were detected (Figs. 5(e, f)).

$$4FePO_4+2Li_2CO_3+C\overset{\Delta}{=\!=}4LiFePO_4+3CO_2\uparrow \quad (3)$$

The evolution of the crystal structures during the regeneration process was studied using in situ XRD measurements. The surfaces of the raw materials were mainly composed of $FePO_4$ (Fig. 6(a)). The diffraction peaks of $FePO_4$ decreased as the roasting temperature increased, indicating a reaction between $FePO_4$, C, and Li_2CO_3 during the regeneration process (Fig. 6(a)). The Rietveld refinement of the XRD data indicates that the XRD spectra of the spent $LiFePO_4$/C did not match well with those of pure $LiFePO_4$/C (PDF#40-1499), suggesting a poor crystal structure in the spent $LiFePO_4$/C, which is consistent with the TEM analysis results.

The diffraction peaks of the regenerated and V-doped regenerated $LiFePO_4$/C well matched that of pure $LiFePO_4$/C, indicating that the regeneration process could restore the crystalline structure of the spent $LiFePO_4$/C (Fig. 6(b)). The lattice parameters of the regenerated $LiFePO_4$/C were nearly the same as the standard data, while those of the V-doped regenerated $LiFePO_4$/C were smaller than the standard and those of the regenerated $LiFePO_4$/C (Table S3 in SM), decreasing the transmission path for Li^+ ions and improving the electrochemical performance of the V-doped regenerated $LiFePO_4$/C materials [45]. This finding is consistent with the results of the EIS analysis. Therefore, the addition of V_2O_5 can enhance the electrochemical performance of the V-doped regenerated $LiFePO_4$/C.

3.3.2 Morphological changes in materials during regeneration process

The morphological changes in the materials during the regeneration process were observed using in situ SEM. Figure S16(a) in SM illustrates that the raw material is composed of granules that

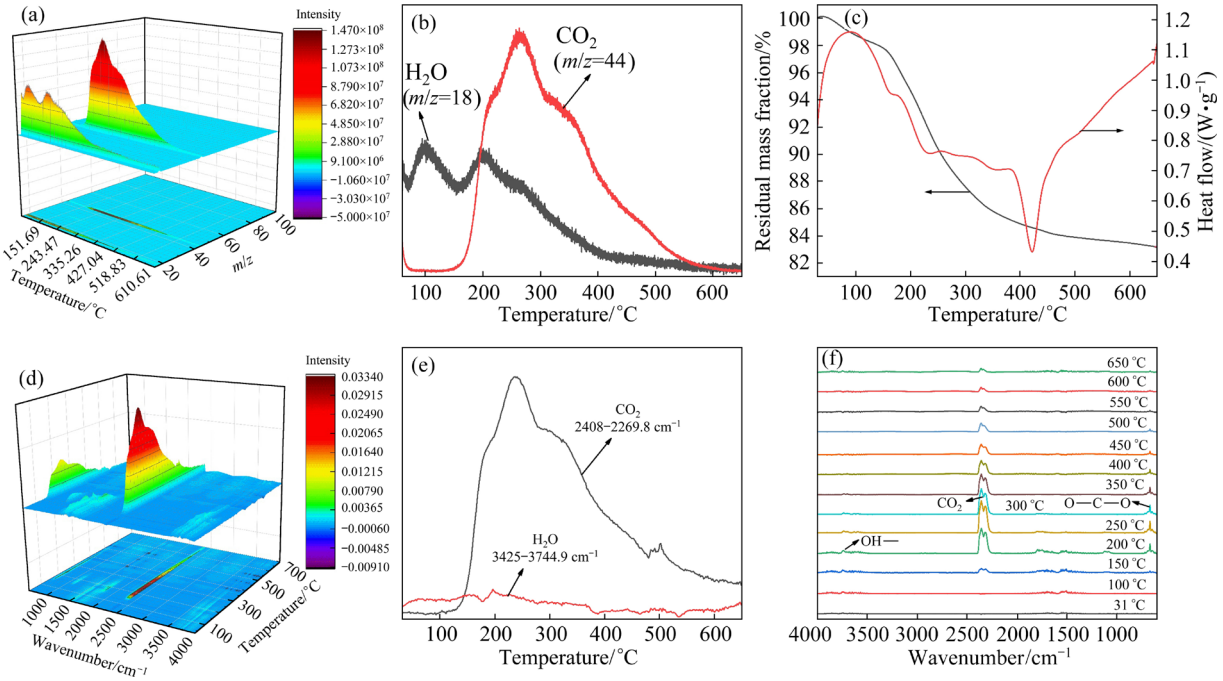

Fig. 5 Analysis results of regeneration process: (a, b) MS spectra and their intensities of gases with obvious peaks; (c) TG−DSC curves; (d, e) FTIR spectra and their intensities at different wavenumbers; (f) FTIR spectra at different temperatures

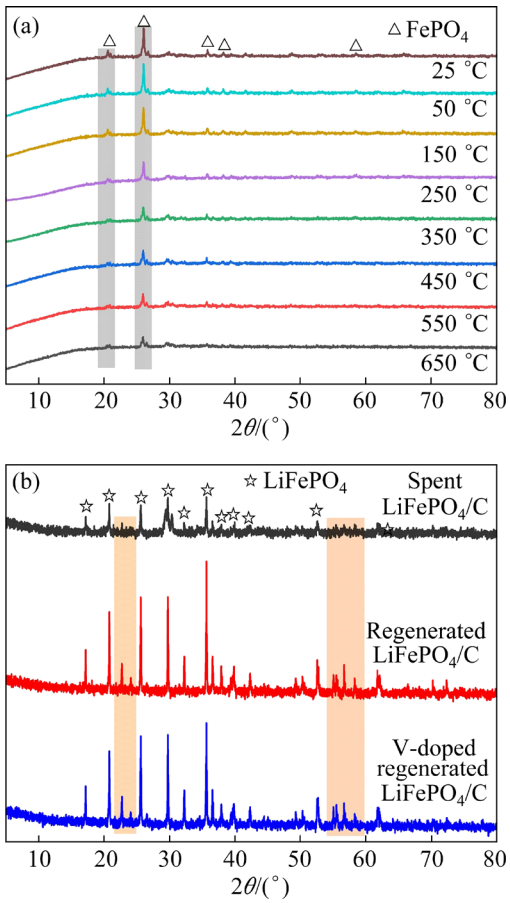

Fig. 6 In situ XRD patterns of regeneration process at different temperatures (a) and XRD patterns of different $LiFePO_4/C$ (b)

are connected by fine floccules. According to the EDS analysis results (Fig. S16(b) and Table S4 in SM), C makes up more than half of the material, while critical elements Fe and P account for 4.53 wt.% and 7.51 wt.%, respectively. The composition may vary in different positions, which is probably due to the difficulty in grinding carbon impurities in spent $LiFePO_4/C$ (Fig. S16 and Table S4). When the roasting temperature is below 250 °C, the floccules melt and adhere to the particle surfaces rapidly (Figs. 7(a−c)). Most of the melted floccules in this process were Glc as the theoretical decomposition temperature of Glc (300 °C) is much lower than that of Li_2CO_3 (618 °C). Consequently, a significant reduction in particle size (Figs. 7(a−c)) and the production of H_2O (Reaction (4) and Fig. 7(d)) occurred, which is consistent with the results of TGA−FTIR−MS.

$$C_6H_{12}O_6 \xlongequal{\Delta} 6C+6H_2O\uparrow \quad (4)$$

When the temperature is above 450 °C, the $LiFePO_4/C$ forms (Reaction (3)), and the spent $LiFePO_4/C$ started to regenerate (Reaction (5), Fig. 7(h)), leading to the slow decrease of particle size and the disappearance of the white Li_2CO_3 attached to the surface of $FePO_4$ and the spent $LiFePO_4/C$ (Figs. 7(d−g)).

$$0.52Li^+ + 0.52e + Li_{0.48}FePO_4 \xlongequal{\Delta} LiFePO_4 \quad (5)$$

The morphological characteristics of the V-doped regenerated $LiFePO_4/C$ were investigated under different regeneration conditions using SEM. The micro floccules between the regenerated V-doped $LiFePO_4/C$ decreased as the roasting time increased from 7 to 10 h (Figs. S17(a−d) in SM). The particles of the V-doped regenerated $LiFePO_4/C$ formed at 750 °C for 11 h have a smooth surface with little floccules among them (Fig. S17(e) in SM). However, when the roasting time was increased to 12 h, the V-doped regenerated $LiFePO_4/C$ particles started to melt together (Fig. S17(f) in SM), resulting in a decrease in the electrochemical performance of the V-doped regenerated $LiFePO_4/C$ (Fig. S12(e) in SM). The SEM images of the V-doped regenerated $LiFePO_4/C$ at different roasting temperatures show that many irregular flocculent substances formed at 600 °C, indicating that this temperature is extremely low for the regeneration of spent $LiFePO_4/C$ (Fig. 8(a)). Elliptical nanoscale particles with a smooth surface formed when the roasting temperature increased to 650 °C, and elements C, O, P, V, and Fe were distributed uniformly, indicating good homogeneity of the V-doped regenerated $LiFePO_4/C$ (Figs. 8(b, c)). However, the particles of the V-doped $LiFePO_4/C$ regenerated at 700, 800, and 900 °C tended to melt together and were larger than those regenerated at 650 °C (Figs. 8(d−f)), which may decrease the electrochemical performance of the V-doped regenerated $LiFePO_4/C$.

3.3.3 Regeneration mechanism

According to the above analysis, the direct regeneration process can be divided into three stages. Firstly, the Glc and Li_2CO_3 were dispersed on the surface of spent $LiFePO_4/C$ and $FePO_4$ when the roasting temperature was low (i.e., 300 °C). The Glc started to decompose when the temperature exceeded 300 °C, resulting in the production of H_2O and C. Some of C was coated on the surface of the regenerated $LiFePO_4/C$, and the remaining C was oxidized with $FePO_4$ to form $LiFePO_4/C$ in the

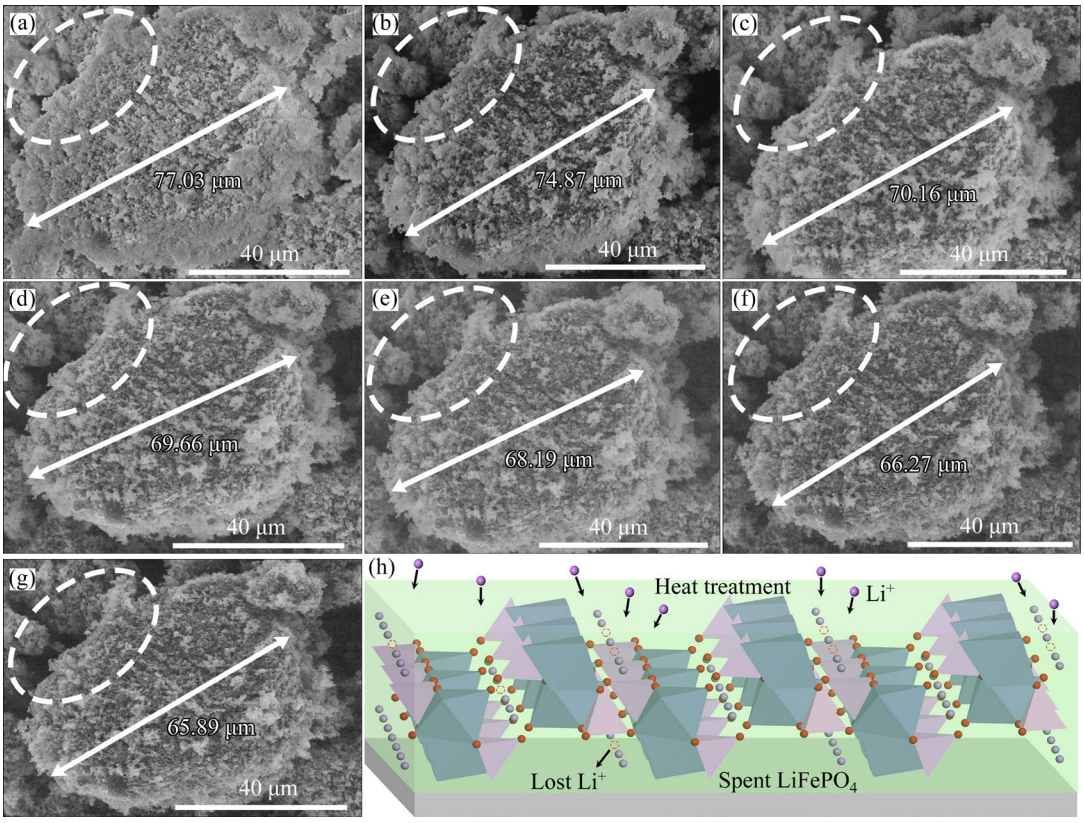

Fig. 7 In situ SEM images of regeneration process at different temperatures: (a) 25 °C; (b) 150 °C; (c) 250 °C; (d) 350 °C; (e) 450 °C; (f) 550 °C; (g) 650 °C; (h) Regeneration of spent $Li_{0.48}FePO_4$

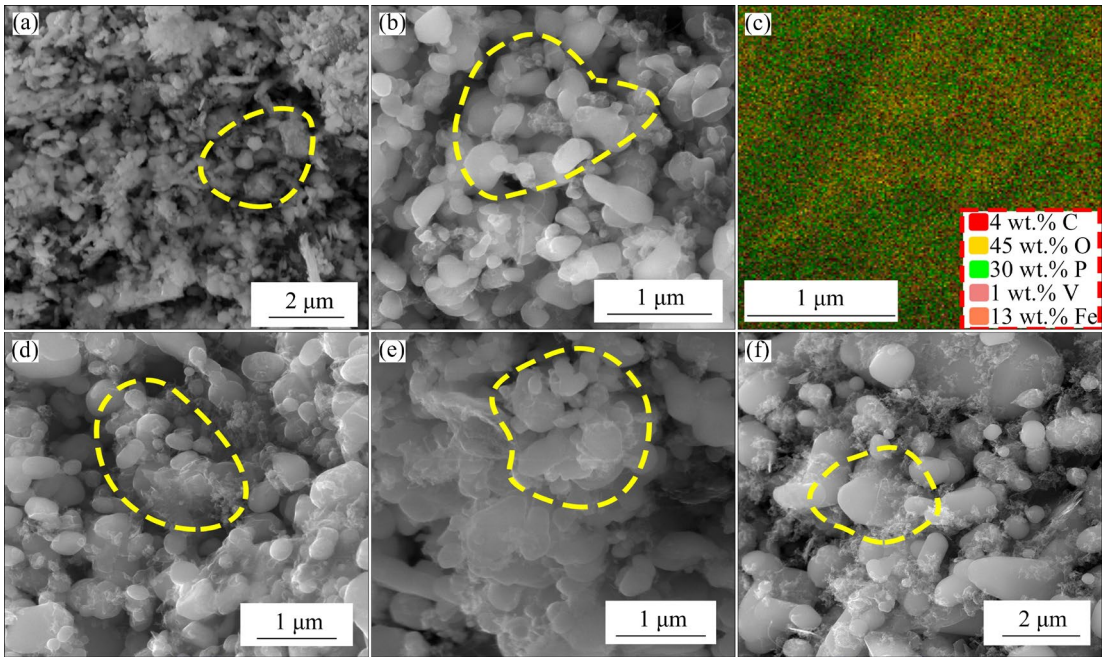

Fig. 8 SEM images of V-doped $LiFePO_4$/C regenerated at roasting time of 11 h and different roasting temperatures: (a) 600 °C; (b) 650 °C; (d) 700 °C; (e) 800 °C; (f) 900 °C; (c) EDS analysis data of (b)

range of 400−650 °C. Thus, the contents of C in the regenerated $LiFePO_4$/C can be regulated by controlling the dosage of Glc and $FePO_4$. The lost lithium and crystal defects in the spent $LiFePO_4$/C can also be replenished and repaired during the direct regeneration process (Fig. 9 and Fig. S14).

The direct recycling process is simpler than the conventional methods. The Al, Cu, shells, and separators present in spent LIBs can be recovered in their most valuable forms. The direct recycling process offers several advantages over other methods, including: (1) simplified operation facilities and processes, (2) reduced operating time, and (3) avoidance of the use of acids (HCl, H_2SO_4, or organic acid) [13].

These advantages contribute to the economic and environmental benefits of the direct regeneration process. For instance, in China, the direct recycling process costs US$16686.86 for 1 t of spent LIBs (the prices of Li_2CO_3, Cu, spent $LiFePO_4$/C, and other agents were based on the market price on April 2, 2023), with approximately 92% of the cost being attributed to the necessary chemicals during the regeneration process. Among these chemicals, Li_2CO_3 incurs the highest cost (US$11071.57) (Table S5 in SM, where the cost of the chemical reagents was based on laboratory experiments, and the cost of electricity, natural gas, and active materials was based on pilot-scale experiments conducted in Shaoshan, Hunan, China). The revenue from the regenerated $LiFePO_4$/C is 27361.20 US$/t, accounting for 95.59% of the total revenues, highlighting the significance of the recycling and regeneration of spent $LiFePO_4$/C batteries (Table S6 in SM and Fig. 10(a)). Furthermore, this direct regeneration process can increase the profitability of the recycling process (11935.44 US$/t) [22] compared with conventional methods (Fig. 10(b)). Therefore, this direct regeneration technology has the potential to facilitate the large-scale disposal of spent $LiFePO_4$/C batteries due to the significant reductions in operation facilities and the profitability of the technological processes.

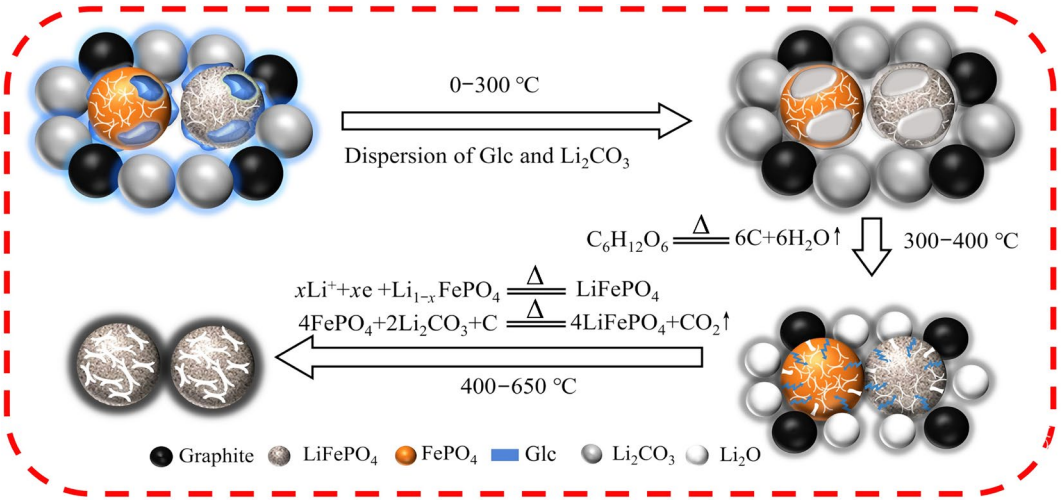

Fig. 9 Schematic diagram of regeneration process

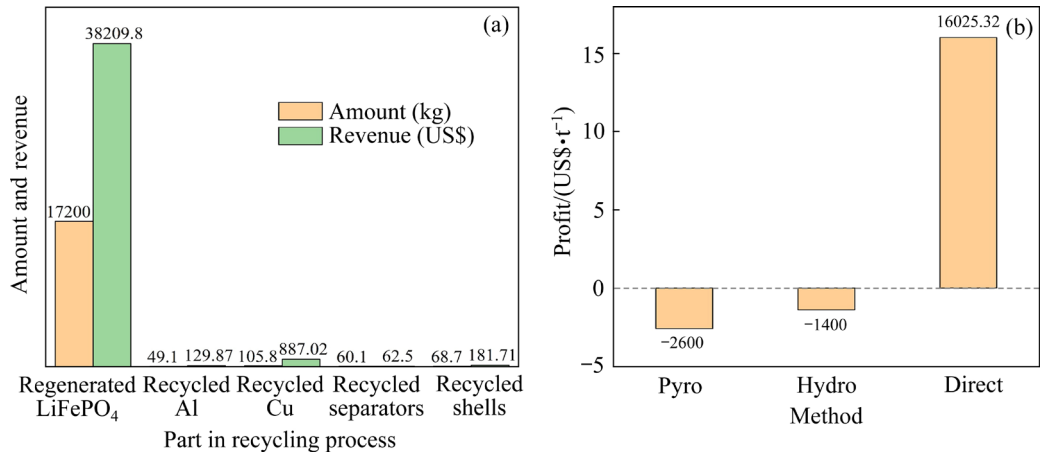

Fig. 10 Amount and revenue from different parts in recycling process (a), and profit of recycling 1 t of spent LIBs with pyrometellurgical ("Pyro"), hydrometallurgical ("Hydro") and direct recycling ("Direct") methods (b) [22]

4 Conclusions

(1) A novel direct regeneration process based on a tunable oxidization and reduction strategy is proposed to regenerate the spent $LiFePO_4$/C cathode material. This strategy aims to eliminate the adverse effects of the inevitable mixing of carbon powder in the spent $LiFePO_4$/C by utilizing an oxidation reaction with the addition of $FePO_4$.

(2) Electrochemical tests reveal that spent $LiFePO_4$/C can be regenerated by roasting at 650 °C for 11 h with the addition of Li_2CO_3, $FePO_4$, V_2O_5, and glucose. The regenerated V-doped $LiFePO_4$/C demonstrates excellent electrochemical performance, which exhibits a discharge specific capacity of 161.36 mA·h/g at 0.2*C*, and the capacity retention after 100 cycles is 97.85%.

(3) The TEM, XPS, SEM, and in-situ XRD tests of the regeneration process indicate that the direct regeneration process can revitalize the electrochemical performance, surface composition, crystal structure, and carbon layer of the spent $LiFePO_4$/C. In situ SEM and electrochemical tests also suggest that the addition of V_2O_5 can improve the cycle performance of regenerated cathode materials, and glucose can revitalize the carbon layers on the surface of the spent $LiFePO_4$/C particles. This innovative technology may pave the way for the large-scale closed-loop recycling of spent $LiFePO_4$/C batteries.

CRediT authorship contribution statement

Xue-hu ZHONG: Conceptualization, Methodology, Formal analysis, Investigation, Writing − Original draft; **Wen-qing QIN:** Resources, Data curation, Funding acquisition; **Jiang ZHOU:** Data Curation, Writing − Review & editing; **Jun-wei HAN:** Conceptualization, Resources, Data curation, Writing − Review & editing, Supervision, Funding acquisition, Project administration.

Declaration of competing interest

The authors declare that they have no known competing financial interests or personal relationships that could have appeared to influence the work reported in this paper.

Acknowledgments

The authors gratefully acknowledge the financial supports from the National Natural Science Foundation of China (Nos. 52174269, 52374293), and the Science and Technology Innovation Program of Hunan Province, China (Nos. 2024CK1009, 2022RC1123).

Supporting Materials

Supporting Materials in this paper can be found at: http://tnmsc.csu.edu.cn/download/23-p0653-2023-0839-Supporting_Materials.pdf.

References

[1] FAN Er-sha, LI Li, WANG Zhen-po, LIN Jiao, HUANG, Yong-xin, YAO Ying, CHEN Ren-jie, WU Feng. Sustainable recycling technology for li-ion batteries and beyond: Challenges and future prospects [J]. Chemical Reviews, 2020, 120(14): 7020−7063.

[2] MY battery network: The global shipment of lithium batteries reached 957.7GWh, and the growth rate of energy storage batteries exceeded that of power batteries [R/OL]. 2022. https://baijiahao.baidu.com/s?id=1755240848988273135&wfr=spider&for=pc

[3] SHANMUKARAJ D, RANQUE P, BEN YOUCEF H, ROJO T, POIZOT P, GRUGEON S, LARUELLE S, GUYOMARD D. Review: Towards efficient energy storage materials: Lithium intercalation/organic electrodes to polymer electrolytes: A road map [J]. Journal of the Electrochemical Society, 2020, 167(7): 070530.

[4] XYLIA M, LEDUC S, LAURENT A B, PATRIZIO P, VAN DER MEER Y, KRAXNER F, SILVEIRA S. Impact of bus electrification on carbon emissions: The case of Stockholm [J]. Journal of Cleaner Production, 2019, 209: 74−87.

[5] WANG Yi-xuan, TANG Bao-jun, SHEN Meng, WU Yi-zhou, QU Shen, HU Yu-jie, FENG Ye. Environmental impact assessment of second life and recycling for $LiFePO_4$ power batteries in China [J]. Journal of Environmental Management, 2022, 314: 115083.

[6] MARKEY B, ZHANG M H, ROBB I, XU P P, GAO H P, ZHANG D W, HOLOUBEK J, XIA D, ZHAO Y F, GUO J C, CAI M, MENG Y S, CHEN Z. Effective upcycling of graphite anode: Healing and doping enabled direct regeneration [J]. Journal of the Electrochemical Society, 2020, 167(16): 160511.

[7] DUAN Xiao-wei, ZHU Wen-kun, RUAN Zhong-kui, XIE Min, CHEN Juan, REN Xiao-han. Recycling of lithium batteries: A review [J]. Energies, 2022, 15(5): 1611.

[8] RAJ T, CHANDRASEKHAR K, KUMAR A N, SHARMA P, PANDEY A, JANG M, JEON B H, VARJANI S, KIM S H. Recycling of cathode material from spent lithium-ion batteries: Challenges and future perspectives [J]. Journal of Hazardous Materials, 2022, 429: 128312.

[9] WU De-you, WANG Dong-xing, LIU Zhi-qiang, RAO Shuai, ZHANG Kui-fang. Selective recovery of lithium from spent lithium iron phosphate batteries using oxidation pressure sulfuric acid leaching system [J]. Transactions of Nonferrous Metals Society of China, 2022, 32(6): 2071−2079.

[10] HUANG Han-lin, LIU Chun-wei, SUN Zhi, Transformation and migration mechanism of fluorine-containing pollutants in the pyrolysis process of spent lithium-ion battery [J].

Journal of Hazardous Materials, 2022, 435: 128974.

[11] GU Kun-hong, GU Xing-yuan, WANG Yong-wei, QIN Wen-qing, HAN Jun-wei. A green strategy for recycling cathode materials from spent lithium-ion batteries using glutathione [J]. Green Chemistry, 2023, 25(11): 4362−4374.

[12] YANG Jian, JIANG Liang-xing, LIU Fang-yang, JIA Ming, LAI Yan-qing. Reductive acid leaching of valuable metals from spent lithium-ion batteries using hydrazine sulfate as reductant [J]. Transactions of Nonferrous Metals Society of China, 2020, 30(8): 2256−2264.

[13] DANG Hui, CHANG Zhi-dong, WU Xue, MA Si-hang, ZHAN Yi-fei, LI Na, LIU Wen-bo, LI Wen-jun, ZHOU Hua-lei, SUN Chang-yan. Na_2SO_4−NaCl binary eutectic salt roasting to enhance extraction of lithium from pyro-metallurgical slag of spent lithium-ion batteries [J]. Chinese Journal of Chemical Engineering, 2022, 41: 294−300.

[14] GU Kun-hong, ZHENG Wei-peng, DING Bo-dong, HAN Jun-wei, QIN Wen-qin. Comprehensive extraction of valuable metals from waste ternary lithium batteries via roasting and leaching: Thermodynamic and kinetic studies [J]. Minerals Engineering, 2022, 186: 107736.

[15] MESHRAM P, MISHRA A, ABHILASH SAHU R. Environmental impact of spent lithium ion batteries and green recycling perspectives by organic acids—A review [J]. Chemosphere, 2020, 242: 125291.

[16] LI Fang-cheng, ZHANG Gang, ZHANG Zong-liang, YANG Jian, LIU Fang-yang, JIA Ming, JIANG Liang-xing. Regeneration of Al-doped $LiNi_{0.5}Co_{0.2}Mn_{0.3}O_2$ cathode material by simulated hydrometallurgy leachate of spent lithium-ion batteries [J]. Transactions of Nonferrous Metals Society of China, 2022, 32(2): 593−603.

[17] ZHANG Jia-feng, HU Wen-yang, ZOU Jing-tian, WANG Xiao-wei, LI Peng-fei, PENG De-zhao, LI Yong, ZHAO Rui-rui, HE Di. Directional high-value regeneration of lithium, iron, and phosphorus from spent lithium iron phosphate batteries [J]. ACS Sustainable Chemical Engineering, 2022, 9(13): 4711−4721.

[18] ZHAO Yan-lan, YUAN Xing-zhong, JIANG Long-bo, WEN Jia, WANG Hou, GUAN Ren-peng, ZHANG Jing-jing, ZENG Guang-ming. Regeneration and reutilization of cathode materials from spent lithium-ion batteries [J]. Chemical Engineering Journal, 2020, 383: 123089.

[19] QIN Zuo-yu, ZHANG Tao, GAO Xue-song, LUO Wu-qing, HAN Jun-wei, LU Bin-an, ZHOU Jiang, CHEN Gen. Self-reconstruction of highly degraded $LiNi_{0.8}Co_{0.1}Mn_{0.1}O_2$ toward stable single-crystalline cathode [J]. Advanced Materials, 2023: 2307091.

[20] HARPER G, SOMMERVILLE R, KENDRICK E, DRISCOLL L, SLATER P, STOLKIN R, WALTON A, CHRISTENSEN P, HEIDRICH O, LAMBERT S, ABBOTT A, RYDER K, GAINES L, ANDERSON P. Recycling lithium-ion batteries from electric vehicles [J]. Nature, 2020, 575(7781): 75−86.

[21] FAN Xiao-ping, TAN Chun-lei, LI Yu, CHEN Zhi-qiang, LI Ya-hao, HUANG You-guo, PAN Qi-chang, ZHENG Feng-hua, WANG Hong-qiang, LI Qing-yu. A green, efficient, closed-loop direct regeneration technology for reconstructing of the $LiNi_{0.5}Co_{0.2}Mn_{0.3}O_2$ cathode material from spent lithium-ion batteries [J]. Journal of Hazardous Materials, 2021, 410: 124610.

[22] XU P P, DAI Q, GAO H P, LIU H D, ZHANG M H, LI M Q, CHEN Y, AN K, MENG Y S, LIU P, LI Y R, SPANGENBERGER J, GAINES L, LU J, CHEN Z. Efficient direct recycling of lithium-ion battery cathodes by targeted healing [J]. Joule, 2020, 4(12): 2609−2626.

[23] JIANG Si-qi, LI Xi-guang, GAO Qiang, LYU Xiao-jun, AKANYANGE S N, JIAO Tian-tian, ZHU Xiang-nan. Review on full-component green recycling of spent lithium iron phosphate cathode materials: From the perspective of economy and efficiency [J]. Separation and Purification Technology, 2023, 324: 124630.

[24] ZHONG Xue-hu, LIU Wei, HAN Jun-wei, JIAO Fen, QIN Wen-qin, LIU Tong. Pretreatment for the recovery of spent lithium ion batteries: Theoretical and practical aspects [J]. Journal of Cleaner Production, 2020, 263: 121439.

[25] ZHONG Xue-hu, LIU Wei, HAN Jun-wei, JIAO Fen, QIN Wen-qin, LIU Tong, ZHAO Chun-xiao. Pyrolysis and physical separation for the recovery of spent $LiFePO_4$ batteries [J]. Waste Management, 2019, 89: 83−93.

[26] ZHONG Xue-hu, LIU Wei, HAN Jun-wei, JIAO Fen, ZHU Hai-ling, QIN Wen-qing. Pneumatic separation for crushed spent lithium-ion batteries [J]. Waste Management, 2020, 118: 331−340.

[27] WANG Tao, YU Xiao-shuang, FAN Min, MENG Qing-hai, XIAO Yao, YIN Ya-xia, LI Hong-liang, GUO Yu-guo. Direct regeneration of spent $LiFePO_4$ via a graphite prelithiation strategy [J]. Chemical Communications, 2019, 56(2): 245−248.

[28] FAN Min, MENG Qing-hai, CHANG Xin, GU Chao-fan, MENG Xin-hai, YIN Ya-xia, LI Hong-liang, WAN Li-jun, GUO Yu-guo. In situ electrochemical regeneration of degraded $LiFePO_4$ electrode with functionalized prelithiation separator [J]. Advanced Energy Materials, 2022, 12(18): 2103630.

[29] SHI Yang, CHEN Gen, CHEN Zheng. Effective regeneration of $LiCoO_2$ from spent lithium-ion batteries: A direct approach towards high-performance active particles [J]. Green Chemistry, 2018, 20(4): 851−862.

[30] LEI Shu-ya, ZHANG Yin-tao, SONG Shao-le, XU Rui, SUN Wei, XU Sheng-ming, YANG Yue. Strengthening valuable metal recovery from spent lithium-ion batteries by environmentally friendly reductive thermal treatment and electrochemical leaching [J]. ACS Sustainable Chemical Engineering, 2021, 9(20): 7053−7062.

[31] XI Xiao-li, CHEN Guang-lei, NIE Zuo-ren, HE Shan, PI Xiong, ZHU Xiao-guang, ZHU Jian-jian, ZUO Tie-yong. Preparation and performance of $LiFePO_4$ and $LiFePO_4$/C cathodes by freeze-drying [J]. Journal of Alloys and Compounds, 2010, 497(1/2): 377−379.

[32] HONG Jian-he, WEI Wen-fei, HE Gang. Optimizing the particle-size distribution and tap density of $LiFePO_4$/C composites containing excess lithium [J]. Ionics, 2019, 25(5): 2035−2039.

[33] JIANG Zhong-qing, JIANG Zhong-jie. Effects of carbon content on the electrochemical performance of $LiFePO_4$/C core/shell nanocomposites fabricated using $FePO_4$/ polyaniline as an iron source [J]. Journal of Alloys and Compounds, 2012, 537: 308−317.

[34] YUE Hai-fang, WANG Dong, ZHU Jian-hua, LI Liao-sha.

Utilizing phosphating sludge to synthesize lithium iron phosphate with a hybrid coating of metal oxides and carbon [J]. ACS Sustainable Chemical Engineering, 2017, 5(4): 3019−3026.

[35] WANG Li, JIAO Chang-mei, LIANG Guang-chuan, ZHAO Nan-nan, WANG Ya-mian, LI Lin-ci. Effect of rare earth ions doping on properties of $LiFePO_4$/C cathode material [J]. Journal of Rare Earths, 2014, 32(9): 895−899.

[36] ZHONG Shu-lin, QIU Jia-hao, LUO Wen-wen, WU Mu-sheng. First-principles study of properties of rare-earth-doped $LiFePO_4$ [J]. Acta Physica Sinica, 2021, 70(15): 158203.

[37] HU Lung-hao, WU Feng-yu, LIN Cheng-te, KHLOBYSTOV A, LI Lain-jong. Graphene-modified $LiFePO_4$ cathode for lithium ion battery beyond theoretical capacity [J]. Nature Communications, 2013, 4: 1687.

[38] WANG Jia-jun, SUN Xue-liang, Olivine $LiFePO_4$: The remaining challenges for future energy storage [J]. Energy & Environmental Science, 2015, 8(4): 1110−1138.

[39] BREDAR A R C, CHOWN A L, BURTON A R, FARNUM B H. Electrochemical impedance spectroscopy of metal oxide electrodes for energy applications [J]. ACS Applied Energy Materials, 2020, 3(1): 66−98.

[40] AURBACH D. Review of selected electrode−solution interactions which determine the performance of Li and Li ion batteries [J]. Journal of Power Sources, 2000, 89: 206−218.

[41] LIU H, LI C, ZHANG H P, FU L J, WU Y P, WU H Q. Kinetic study on $LiFePO_4$/C nanocomposites synthesized by solid state technique [J]. Journal of Power Sources, 2006, 159(1): 717−720.

[42] ALEXANDER V, NAUMKIN A K V, STEPHEN W, GAARENSTROOM C J P. NIST X-ray photoelectron spectroscopy database [EB/OL]. 2000−06−06.

[43] XU Fan, HE Hao, LIU Ya-dong, DUN C, REN Yang, LIU Qi, WANG Mei-xian, XIE Jian. Failure investigation of $LiFePO_4$ cells under overcharge conditions [J]. Journal of the Electrochemical Society, 2012, 159(5): A678−A687.

[44] HE Li-hua, LIU Xu-heng, ZHAO Zhong-wei. Non-isothermal kinetics study on synthesis of $LiFePO_4$ via carbothermal reduction method [J]. Thermochimica Acta, 2013, 566: 298−304.

[45] CHEN Ya-wen, CHEN Jenn-shing. A study of electro-chemical performance of $LiFePO_4$/C composites doped with Na and V [J]. International Journal of Electrochemical Science, 2012, 7(9): 8128−8139.

可调控氧化还原策略直接修复再生废旧锂电池正极材料

钟雪虎[1]，覃文庆[1]，周 江[2]，韩俊伟[1]

1. 中南大学 资源加工与生物工程学院，长沙 410083；
2. 中南大学 材料科学与工程学院，长沙 410083

摘 要：提出一种通过添加 $FePO_4$ 氧化多余碳的可调控氧化还原方法对废旧 $LiFePO_4$/C 正极材料进行直接修复再生。修复再生试验表明，将废旧 $LiFePO_4$/C 正极材料与一定量的 Li_2CO_3、$FePO_4$、V_2O_5 及葡萄糖混合后，将混合料在 650 ℃下焙烧 11 h 修复后就能得到具有较好性能的正极材料。添加 V_2O_5 能够提高修复再生后 $LiFePO_4$/C 正极材料的循环性能，葡萄糖则通过修复 $LiFePO_4$/C 表面包覆碳层来提高修复再生后 $LiFePO_4$/C 的导电性。修复再生后钒掺杂 $LiFePO_4$/C 正极材料表现出优异的电化学性能，在 0.2*C* 倍率下的放电比容量为 161.36 mA·h/g，100 次循环后容量保持率为 97.85%。

关键词：废旧锂电池；直接修复再生；正极材料；焙烧；循环经济

(Edited by Wei-ping CHEN)